SPARK HEAT TRANSFER MEASUREMENTS IN FLOWING GASES*

D. VERHOEVEN

Institut français du pétrole[1]

RÉSUMÉ DES TRANSFERTS DE CHALEUR ENTRE UNE ÉTINCELLE D'ALLUMAGE ET DES ÉCOULEMENTS GAZEUX

À partir de techniques basées sur l'interférométrie holographique, l'énergie totale transférée par une étincelle aux gaz environnants a été mesurée en faisant varier la géométrie des électrodes de la bougie d'allumage, la vitesse des gaz, la pression et le temps de charge de la bobine, cette dernière étant un modèle standard pour automobile.

Pour les différentes combinaisons et valeurs des paramètres étudiés, il a été observé une variation du "rendement d'étincelle" (rapport entre l'énergie transmise aux gaz par l'étincelle à l'énergie électrique fournie à la bougie) allant de 20 à 60 %. Pour des conditions réelles de fonctionnement dans un moteur, on peut estimer que l'énergie transmise aux gaz par le système d'allumage est voisine de 30 mJ. Il est aussi montré comment ces mesures de l'énergie totale transférée aux gaz, peuvent être exploitées pour caractériser en fonction du temps, la puissance transmise dans l'étincelle générée par un système standard d'allumage inductif.

SPARK HEAT TRANSFER MEASUREMENTS IN FLOWING GASES

Using a technique based on holographic interferometry, the total energy transferred from a spark to the surrounding gases was measured for a number of spark plug electrode geometries, flow velocities, gas pressures and coil charge times. A standard automotive ignition coil was used.

For the combinations of parameter values studied, we observed "spark efficiencies" (ratio of the energy in the gas heated by the spark to the electrical energy supplied to the spark plug) of from 20 to 60 percent. For realistic engine conditions we estimate the quantity of energy transferred to the gas by our ignition system to be roughly 30 mJ. We show how these measurements of total energy transferred to the gas can be used to estimate the spark power vs. time characteristic of a standard inductive ignition system.

MEDICIÓN DE LAS TRANSFERENCIAS DE CALOR ENTRE UNA CHISPA DE ENCENDIDO Y LOS FLUJOS GASEOSOS

Tomando como punto de partida las técnicas fundadas en la interferometría holográfica, se ha procedido a la medición de la energía total transferida por una chispa a los gases circundantes, haciendo variar la geometría de los electrodos de la bujía de encendido, la velocidad de los gases, la presión y el tiempo de carga de la bobina, correspondiendo está última a un modelo estándar para automóvil.

Se ha observado, para las distintas combinaciones y valores de los parámetros estudiados, una variación del "rendimiento de la chispa" (relación entre la energía transmitida a los gases por la chispa a la energía eléctrica suministrada a la bujía) que oscila entre un 20 y un 60 %. Operando en condiciones reales de funcionamiento de un motor, se puede considerar que la energía transmitida a los gases por el sistema de encendido, se aproxima de los 30 mJ. También se indica cómo estas mediciones de la energía total transferida a los gases pueden ser aprovechadas para caracterizar, en función del tiempo, la potencia transmitida en la chispa generada por un sistema estándar de encendido inductivo.

(1) 1 et 4, avenue de Bois-Préau,
92852 Rueil-Malmaison Cedex - France

* This article was presented at the SAE Fuels and Lubricants Meeting and Exposition, Toronto, October 16-19, 1995.

INTRODUCTION

Previous studies have shown the importance of the initial phases of combustion on the stability, efficiency and emissions of internal combustion engines [1-4]. The geometry of the spark plug and characteristics of the ignition system play important roles in the initiation of combustion. This is particularly true in lean-burn engines or those with high EGR rates [5-9]. The physics of the energy transfer from the spark to the surrounding gas and of the initiation of a self-sustaining combustion reaction in the gas are complex. Maly [6] and Kalghatgi [10] give detailed descriptions of these processes. The goal of this work was not to study these phenomena in detail but to provide values for the total thermal energy transferred from the spark to the gas under conditions as close as possible to those in an engine. These data are needed for numerical models of the initiation process.

Recent computer models [11-13] model the spark simply as a source of thermal energy and so require only a value of the total energy supplied by the spark to the gas, or, at most, the power supplied to the gas by the spark as a function of time. This information is usually obtained from published experimental data [14] and [15] measured by calorimetric techniques [16, 17, 18]. A drawback of these techniques is that it is not possible to study with them the spark efficiency in a flowing gas. In this study we used an interferometric technique to measure the energy transferred from the spark to the gas. We present here the measurement technique and results of measurements with various flow speeds at the spark-plug electrodes, pressures, coil charge times, electrode geometries and gas compositions. We also show that with measurements of the total energy transferred to the gas as a function of coil charge time, one can estimate the quantity of energy transferred from the spark during the arc and glow phases of the spark.

1 EXPERIMENTS

1.1 Ignition system

The ignition system is shown schematically in Figure 1. The coil with integrated control electronics was a standard Renault part (part number 7700852662/ S102030002A). On the coil's secondary side were large cross-section copper wires with negligible resistance, and a 1.65 ohm resistor used to determine the secondary current.

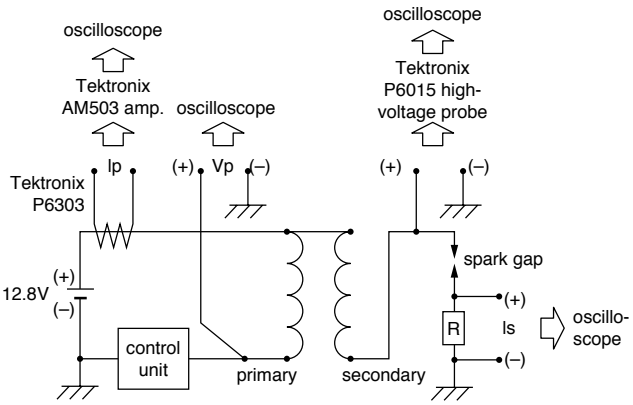

Figure 1

Schematic of ignition system.

The charging characteristic curves of the primary side of the coil are shown in Figure 2.

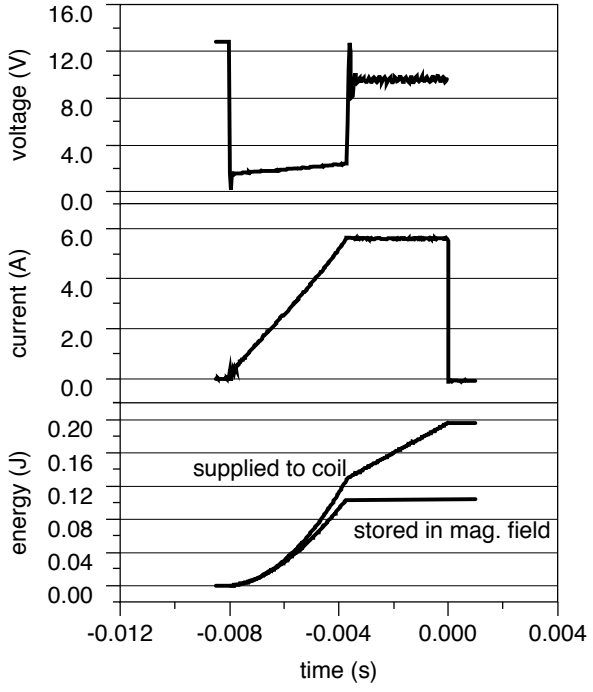

Figure 2

Voltage, current and energy supplied to the primary side of the coil for 8 millisecond charge time.

The control electronics of the coil limited the primary current to 5.5 amperes, which was reached after 4.25 milliseconds. The upper energy curve of Figure 2 gives the integral of the product of the voltage and current, the lower curve gives this integral minus the resistive losses in the winding, i.e. the part of the supplied energy which is stored in the magnetic field of the coil. For the coil charge times used during this study, the energy values are given in Table 1.

TABLE 1

Energy stored in magnetic field of coil

Charge time [ms]	1.5	2.0	3.0	4.0
Energy [mJ]	16	28	56	93

Typical voltage, current and energy curves for the secondary winding are given in Figure 3.

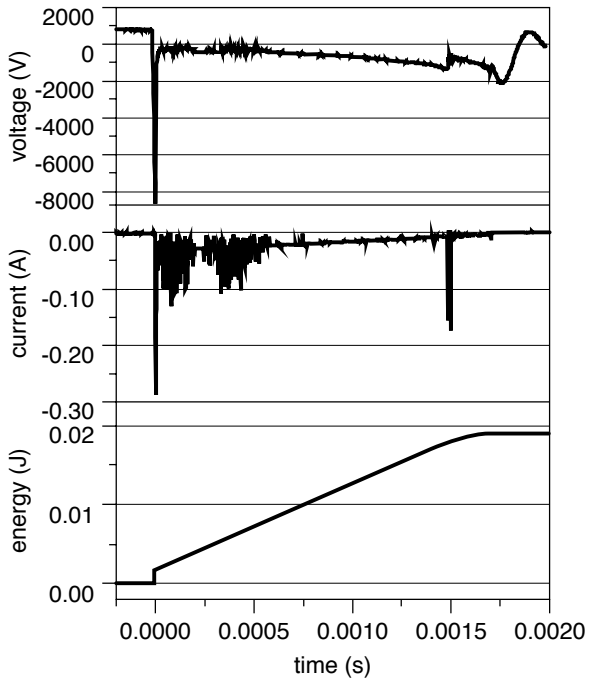

Figure 3

Voltage, current and energy supplied to the spark by the coil's secondary winding. Coil charge time 2 ms, electrode diameter 2.0 mm, gap 1.0 mm, 3.8 m/s flow at gap.

The voltage and current waveforms start with a short peak lasting around 10 microseconds (the "arc" phase) followed by a phase lasting roughly 2 milliseconds characterised by increasing voltage and decreasing current (the "glow" phase). During the glow phase, the discharge is often interrupted and re-struck. These secondary discharges are more frequent the higher the gas velocities in the spark gap.

1.2 Electrical measurements

The current in the coil's secondary winding was computed from the voltage drop across a resistor (R = 1.65 ohms) inserted in the secondary circuit. The secondary voltage was measured through a Tektronix P6015 high voltage probe. The primary side current was measured with a Tektronix P6303 inductive current probe and AM503 amplifier. The probe signals were recorded with a Tektronix TDS400 digital oscilloscope at from 1 to 2.5 × 10^6 samples per second. At these sampling rates, the oscilloscope achieves 11-12 bit resolution using an oversampling and smoothing technique. The initial breakdown discharge for the spark of Figure 3 is shown in Figure 4.

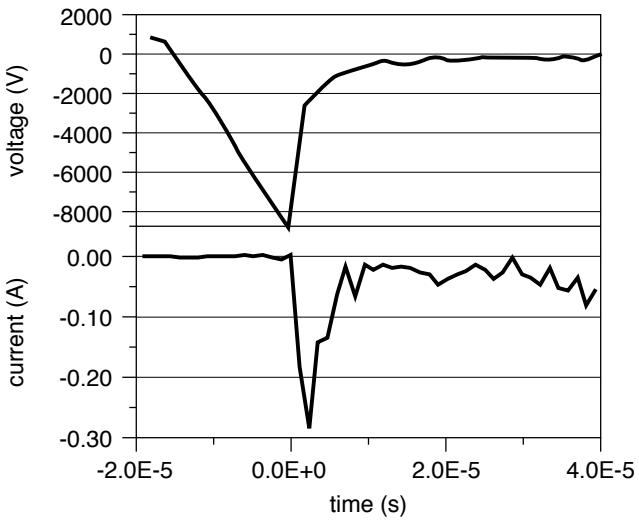

Figure 4

Voltage and current curves for breakdown phase. Same data as Figure 3.

The initial current spike is apparently undersampled. If the sampling rate is increased, structure appears in the signal which at lower sampling rates is smoothed by the oscilloscope.

For instance, at high sampling rates the initial spike corresponding to the breakdown phase of the spark appears, with currents exceeding 25 amperes. Because of the high sampling rate required and the limited dynamic range and memory of the oscilloscope it was not possible for us to record this phase of the discharge accurately. The abrupt rise in the energy curve at the beginning of the spark (Fig. 3, bottom) is therefore underestimated in our measurements, and we cannot give an estimate of the accuracy of the arc-phase electrical measurements. In the results presented below the energy computed for the arc phase is reported separately from that of the glow phase. The absolute accuracy of the reported glow-phase electrical energy measurements is estimated to be ± 3%.

1.3 Optical measurements

The energy transferred to the gas surrounding the spark was measured interferometrically with a phase-stepping holographic interferometer (Fig. 5).

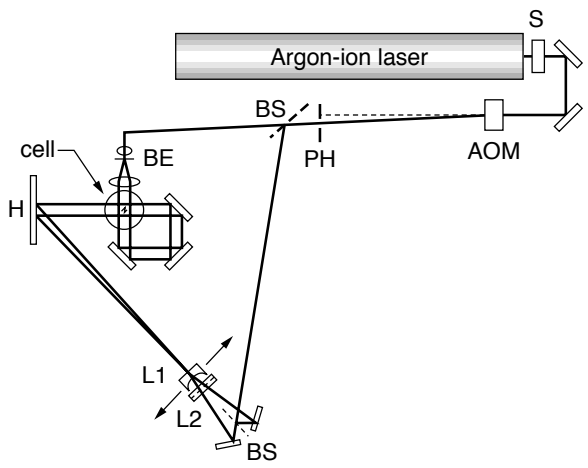

Figure 5

Holographic interferometer used for the energy-transfer measurements. S:shutter; AOM: acousto-optic modulator; PH: pinhole; BS: beamsplitter; BE: beam expander; L: cylindrical lens; H: holographic recording plate. Lens L1 may be shifted as indicated to change the optical phase relationship between the two reference beams [21]. The measurement volume is at the center of the cell.

The beam from an argon laser (λ = 512 nanometers) passes through a mechanical shutter and then through an acousto-optic modulator used as a high-speed shutter. The beam is split into object and reference legs. The object beam is spatially filtered, expanded, collimated and directed twice through the measurement volume at the center of a transparent cell. The double-pass design doubles the sensitivity of the interferometer. The reference beam is split into 2 separate beams which are expanded and directed onto the holographic recording plate where they combine with the object beam. The holographic plate was mounted on a traverse mechanism so that up to 10 holograms could be recorded on a single plate.

To record an interferogram of the gas heated by the spark, a hologram of the object beam is first recorded on the plate using one of the reference beams. A spark is then created in the measurement volume and a second hologram of the object beam is recorded using the other reference beam. The second hologram records the perturbations of the object beam due to the heated gas.

After the holographic plate is developed, it is re-illuminated with both reference beams at once. The two recorded object wavefronts are reconstructed and interfere to produce a pattern of fringes from which the energy information which is sought may be extracted (Fig. 6). This fringe pattern may be digitized with a CCD camera and processed as described below.

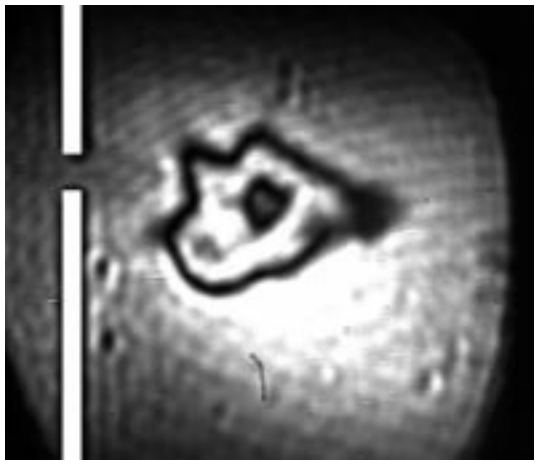

Figure 6

Interferogram of gas heated by spark. The position of the 0.5 mm diameter spark plug electrodes is indicated by the white bands at the left of the image. Note that the shadows of the electrodes from the two passes of the object beam through the measurement volume are superimposed. The gas (air) is flowing at 3.8 m/s.

The light intensity distribution in a fringe pattern may be described by:

$$I(x,y) = I_0(x,y)\left[1 + m(x,y)\cos\left(\Delta\varphi_s(x,y)\right)\right] \quad (1)$$

where $I_0(x, y)$ is the background intensity and m(x, y) is the local fringe contrast. The optical phase difference $\Delta\varphi_s(x,y)$ is related to the heating of the gas by:

$$\Delta\varphi_s(x,y) = \frac{2\pi}{\lambda}\int_s \left(n_2(x,y,z) - n_1(x,y,z)\right)ds \quad (2)$$

where n_2 and n_1 represent the index of refraction in the gas after and before the spark. The integration is carried out along the path of the ray of the object beam corresponding to the position x, y in the fringe pattern (Fig. 7).

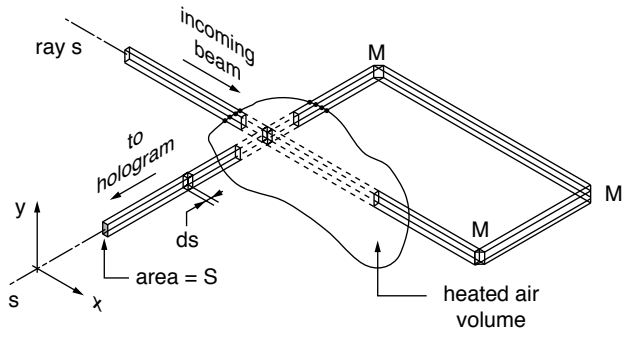

Figure 7

Path of integration for energy computation from interferogram. The object beam is directed twice through the heated gas by three mirrors (M).

The index of refraction may be related to the density, ρ, and hence to the temperature in the gas through the Gladstone-Dale equation:

$$(n - 1) = K_{GD}\rho \quad (3)$$

K_{GD} is a constant related to the composition of the gas and the wavelength of the probing light.

Equation (1) relates the light intensity at each point in the interferogram's pixel pattern to the phase shift undergone by a ray passing through the heated gas. It is, however, difficult to use directly because for each point there are three unknowns ($I_0(x,y)$, $m(x,y)$, and $\Delta\varphi(x,y)$) and only one measurement ($I(x,y)$). This difficulty is overcome by using a phase-stepping, or quasi-heterodyne technique [19] and [20]. Three images of the fringe pattern are recorded with different relative phases of the two reconstructing reference beams. For relative phase shifts of 120 degrees $\Delta\varphi_s(x,y)$ is then derived from:

$$\Delta\varphi'_s(x,y) = \text{atan}\left(\frac{\sqrt{3}\left(I_3(x,y) - I_2(x,y)\right)}{2I_1(x,y) - I_2(x,y) - I_3(x,y)}\right) \quad (4)$$

where the subscripts refer to the three images. This process is illustrated in Figure 8 which shows three phase-shifted images and the image resulting from application of equation (4). Because of the periodicity of the arc tangent function this image ($\Delta\varphi'(x,y)$) has jumps which must be "unwrapped" to obtain the optical phase at each point ($\Delta\varphi(x,y)$, the last image of Figure 8.

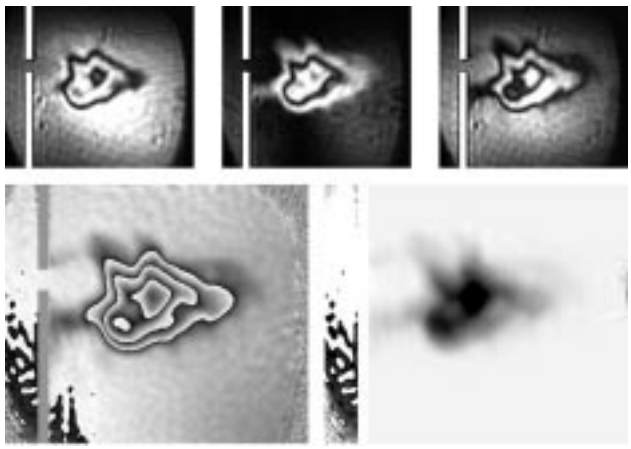

Figure 8

Top: three phase-shifted images of an interferogram. Bottom left: image obtained by application of equation (4) to the images at the top. Bottom right: "unwrapped" image of optical phase distortion of the object beam.

Each pixel of this image gives the change in phase of a ray passing through the measurement volume. The quantity, dE, of energy deposited by the spark in an elementary volume S·ds (after expansion due to heating, see Figure 7) is given by:

$$dE = dU + PdV = dH = C_p\left(T_2 - T_1\right)\rho_2 S ds \quad (5)$$

where Cp is the constant-pressure specific heat of the gas, T_2 the temperature after and T_1 the temperature before the spark. The total energy due to the spark contained in the parallelepiped of cross-section S following the path s is obtained by integration of this quantity along s:

$$E_s = -\frac{CpMPST_1}{R_u}\int_s\left(\frac{1}{T_2}-\frac{1}{T_1}\right)ds \qquad (6)$$

where the ideal gas law has been used to eliminate ρ from equation (5). R_u is the universal gas constant, M the molecular weight of the gas, and P the pressure. Combination of equation (3) with the ideal gas law results in:

$$n_2 - n_1 = \frac{K_{GD}MP}{R_u}\left(\frac{1}{T_2}-\frac{1}{T_1}\right) \qquad (7)$$

which, when combined with equation (6) and equation (2), results in the following expression for the total energy due to the spark in the heated gas:

$$E_{opt} = -\frac{C_pST_1\lambda}{4\pi K_{GD}}\sum_{image}\Delta\varphi_s \qquad (8)$$

The summation in equation (8) can be taken over all the pixels of a digitized image like that of Figure 8, in which case S is equal to the area of one pixel in object-space coordinates. Note that the double passage through the measurement volume has been accounted for in equation (8) by division by 2. This equation was used to compute the "optically-measured" spark energy values reported in the following section.

The accuracy of this technique depends essentially on the accuracy of the optical phase measurement, which is influenced by a number of possible errors. These errors can be minimized by careful choice of techniques and careful experimental work [23]. In this study, the errors were probably dominated by inaccuracies in the background "tilt" correction and interpolation necessary in processing the interferograms. Interpolation was necessary in the measurements made without flow because the spark-heated gas remains around the electrodes, and the shadow of the electrodes masks a portion of the measurement volume. In this situation, we used a linear interpolation from the phase shift values measured on one side of the electrodes to that measured on the other side.

The problem of background tilt can be seen in the lower left image of Figure 8: the undisturbed background which should be of constant (zero) value decreases from the left to the right of the image, probably because of a slight movement of the optics of the interferometer between the recording of the hologram and its reconstruction. Three rows of data extracted from these images are shown in Figure 9.

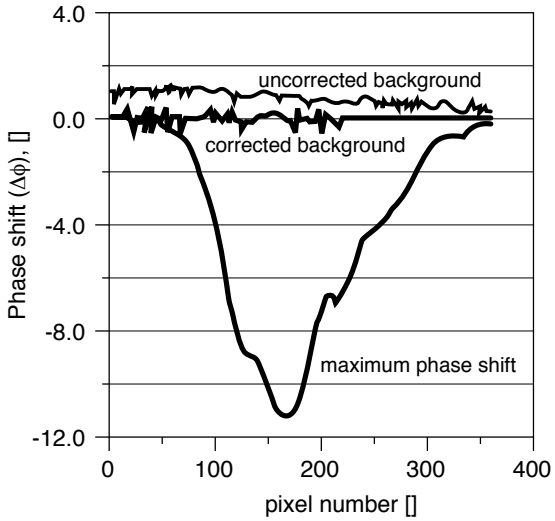

Figure 9

Data extracted from images of Figure 8. The corrected and uncorrected background data were taken from different rows just above the phase disturbance in the lower right and lower left images of Figure 8. The maximum phase shift data were taken from the row of the unwrapped phase image which passes through the maximum of the phase disturbance.

The uncorrected background has an average error of somewhat less than 1 radian. This error can be modelled as a linear function of the two spatial coordinates of the image $\Delta\varphi_{err} = a_0 + a_1(x-x_0) + a_2(y-y_0)$. Fitting this equation to the background areas of the image and subtracting it from the entire image eliminates the background tilt and results in data like the "corrected background" and "maximum phase shift" rows of Figure 9. The rms error of the (non-zero) "corrected background" data is 0.1 radians (0.016 wavelengths).

If we assume a constant phase measurement error of this magnitude over the entire disturbed area of the interferogram (area, S, = 4.3×10^{-5} m^2), equation (8) may be used to compute the energy error. This

computation gives a value of 0.24 mJ, which is 3 percent of the 8.1 mJ total energy measured for this case. This value gives a rough idea of the accuracy of the optical measurement results presented below.

2 EXPERIMENTAL CONDITIONS

A summary of the experimental conditions is presented in Table 2. All experiments were done at room temperature.

TABLE 2

Experimental conditions. Empty cells are to be filled with the values of the base condition

Names ⇓	Dia. (mm)	Gap (mm)	Charge (ms)	Speed (m/s)	Gas	Press. (bar)
Base	2.0	1.0	2.0	3.8	air	1
Diam.	0.5, 1.5					
Gap		2.0, 3.0				
Charge			1.5, 3.0			
Speed				0, 1.9, 5.8		
Gas				0	N_2+16% C_3H_8	
Press				0		2, 3, 4, 5, 6

Note that there was no flow in the experiments which were done with air pressures from 2 to 6 bars and those done in a mixture of nitrogen and propane (at 1 bar).

The spark plug electrodes were made of 304L stainless steel. Both electrodes were cylindrical and extended to the center of the measurement cell (Fig. 6). Experiments were done at atmospheric pressure to assess the effect of the electrodes' surface condition on the spark; no significant effect was observed.

The flow for these experiments was produced by a 25 millimeter nozzle placed 60 millimeters from the electrodes. Velocity profiles in the plane of the electrodes along a diameter of the air jet are shown in Figure 10.

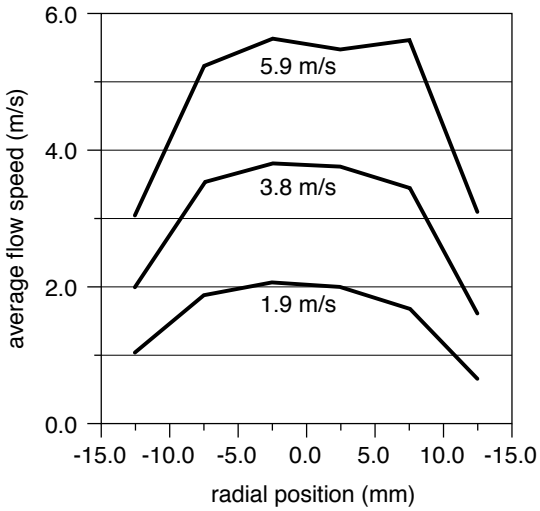

Figure 10

LDV measurements of air speeds in the plane of the electrodes. Speed designations used in this paper refer to values computed from the measured flow rate and the nozzle diameter.

For experiments done at 1 bar, the holograms were recorded from 1 to 5 milliseconds after the end of the spark. For higher pressures (without flow) delays of several tens of milliseconds were necessary to allow the thermal energy to diffuse away from the electrodes.

If the hologram was recorded too soon after the spark we encountered ray-crossing problems because of the strong thermal gradients in the gas [22]. The exposure time used for the hologram recording was between 100 and 200 microseconds.

3 RESULTS

The experimental results are summarized in Table 3. Selected results from this table and results for measurements made without flow are presented in Figures 11 through 14.

The data in these figures represent the average E_{opt} from Table 3, the "error" bars extend 2 standard deviations above and below the mean values and give an idea of the variability of the sparks.

The electrical energy supplied to the electrodes depends almost only on the coil charging time (Table 3, E_t). Except for Figure 11 in which the charge time was varied, one may therefore interpret the ordinates of

these plots as spark efficiencies, which may be computed from the ordinate value divided by the electrical energy supplied to the spark plug (which was roughly 18 mJ in all 2 ms coil charge cases).

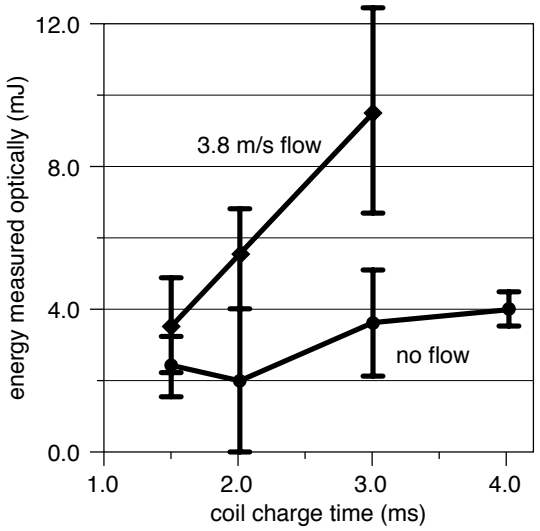

Figure 11

Energy transferred to gas as a function of the coil charge time and flow (in air). Electrode gap: 1.0 mm; diameter: 2.0 mm; P: 1 bar; see Table 3 for electrical energy supplied to electrodes.

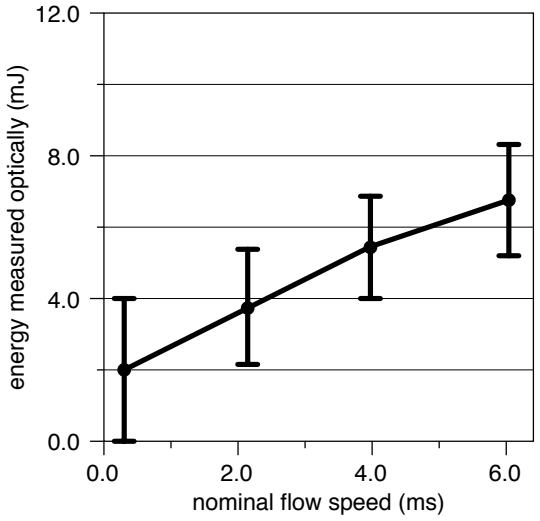

Figure 12

Energy transferred to gas as a function of the nominal flow speed at the electrodes. Electrode gap: 1.0 mm; diameter: 2.0 mm; P: 1 bar; approximately 18 mJ electrical energy supplied to electrodes.

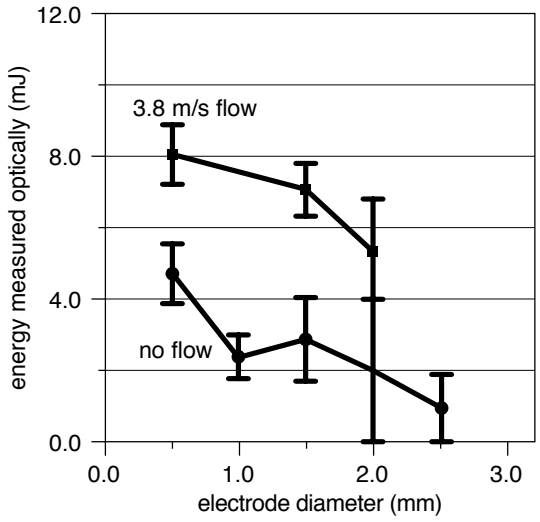

Figure 13

Energy transferred to gas as a function of the electrode diameter and flow (in air). Electrode gap: 1.0 mm; P: 1 bar; approximately 18 mJ electrical energy supplied to electrodes.

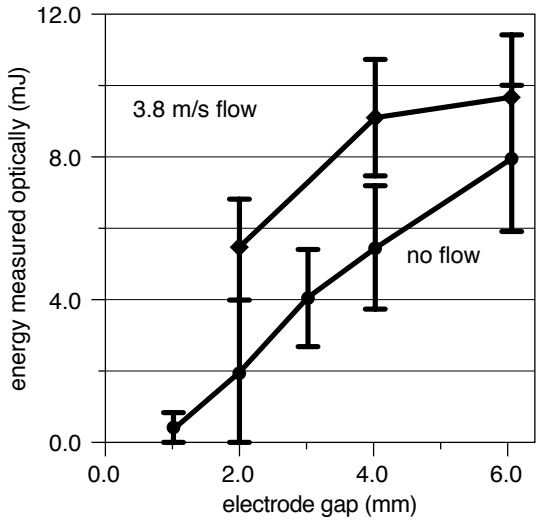

Figure 14

Energy transferred to gas as a function of the electrode gap and flow (in air). Electrode diameter: 2.0 mm; P: 1 bar; approximately 18 mJ electrical energy supplied to electrodes.

4 DISCUSSION

4.1 Spark effficiency

The results show clearly the strong effect of the flow on the energy transfer efficiency of the spark. Figure 12 shows that a flow speed of 2-3 meters per second is sufficient to double the efficiency with respect to that in

a quiescent gas. The effect of the electrode geometry is similar with and without flow: the efficiency drops sharply with increasing electrode diameter and decreasing gap. The energy transfer efficiencies measured without flow are considerably higher than those reported previously. For example, Teets and Sell [14] measured, using calorimetric techniques, an efficiency of 13 ± 2% for a "standard" spark plug with 2 mm gap, and Saggau [15] gives an efficiency value of about 13% for 2.5 mm diameter stainless steel electrodes with a 2 mm gap. We measured an efficiency of 26% for 2 mm diameter, 2 mm gap electrodes. All these measurements were made without flow, at 1 bar, in air, with similar ignition systems.

A possible explanation for the higher efficiencies measured during this study lies in the observed variability of the sparks when there is no flow. During our experiments without flow it was clear that there were (at least) two classes of sparks, which could be distinguished by their loudness as well as the electrical and optical measurement data. The different sparks occurred in runs. Figure 15 shows data from two series of measurements made successively under the same conditions: the average arc-phase electrical energy is 5 times greater for one series, while the energy transferred to the gas is 3 times greater. One series consisted entirely of "weak" sparks, the other entirely of "strong" ones. It is not clear what the physical basis for this difference is. It could explain the higher efficiencies observed during this study because a large percentage of our measurements (90%) are for "strong" sparks. A second example of this phenomenon can be seen in Figure 13: the experiments done with 1 millimeter diameter electrodes and no flow had a particularly large percentage of weak sparks. This phenomenon was not observed in experiments made with an air flow at the electrodes and so it is of little practical importance.

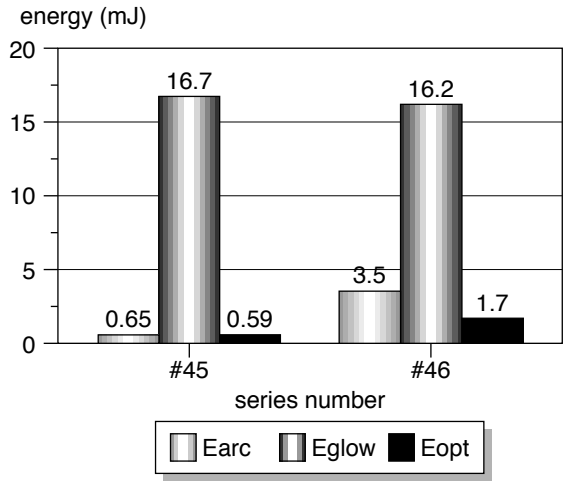

Figure 15

Average energies for two series of 8 measurements made under identical conditions: no flow, 1 bar, in air, 2.0 mm diameter, 1.0 mm gap electrodes.

4.2 "Engine" conditions

Although it is possible to study spark efficiencies in conditions close to those of a motor (simultaneous flow and higher-than-atmospheric temperatures and pressures) with the measurement technique presented here, we were not equipped to do so. We can, however, estimate the amount of energy transferred to the gas under such conditions based on the assumption that the effects of the aero- and thermodynamic conditions are independent. This assumption may be justified by the fact that these conditions affect the energy transfer through different physical phenomena: the flow reduces the energy losses to the electrodes by moving the plasma and the heated gas away from them and by shortening the discharge duration, while increasing the gas pressure both increases the breakdown voltage, and hence the arc phase energy, and decreases the thermal diffusivity of the gas.

In air at 1 bar, 300 K with a coil charge time of 4 milliseconds (about 50 millijoules coil secondary energy) we estimate the quantity of energy transferred to the gas to be 13 millijoules (Fig. 11: 2 millimeter diameter electrodes, 1 millimeter gap, 3.8 meter/second flow). Increasing the pressure from 1 to 5 bars increases the energy transferred by a factor of roughly 2.5 (Table 3). This would result in around 30 millijoules in the gas or an efficiency of 60%. We did not investigate experimentally the effect of the gas temperature on the energy transfer. Higher temperatures strongly increase the thermal diffusivity of the gas and would therefore increase the overall energy transfer from the spark, but by how much is not known.

4.3 Spark power

It is often useful to know what part of the spark energy is transferred to the gas during the arc and glow phases of the spark. While the technique presented here measures directly only the total energy transferred to the gas, these measurements can be used to estimate the individual contributions of the arc and glow phases. If we express the quantity of energy transferred to the gas (which is that measured optically, E_{opt}) as:

$$E_{opt} = \eta_{arc} E_{arc} + \eta_{gl} E_{gl} \quad (9)$$

i.e. as the sum of the electrical energies supplied to the spark plug multiplied by energy transfer efficiencies, h, then from the measured values of E_{opt}, E_{arc} and E_{gl} for a number of different conditions we can estimate the values of η. E_{arc} and E_{gl} may be varied by changing the charge time of the ignition coil (Table 3). We assume that this variation does not change the energy transfer efficiencies. Using the results of the 23 "charge" experiments of Table 3 and minimizing the squared error of equation (9), one obtains $\eta_{arc} = 0.33$ and $\eta_{gl} = 0.30$ for air at 1 bar, 3.8 meters per second flow, with 2 mm diameter, 1 mm gap electrodes. For the same conditions without flow, one obtains the values

TABLE 3

Top: results for experiments with flow, bottom: without flow. Asterisks indicate parameter values of the base condition (see Table 2 for conditions corresponding to names at left). N: number of measurements; E_{opt}: energy measured in gas measured optically; E_{arc}: electrical energy supplied to the spark plug during the first 14 microseconds of the spark discharge; E_{gl}: electrical energy supplied to the spark plug during the glow phase of the spark; dur.: duration of spark; E_t: $E_{arc} + E_{glow}$; η_p: E_t / E_{mag} where E_{mag} is the energy stored in the magnetic field of the coil; η_s: E_{opt} / E_t

			Averages							Standard deviations			
Name	Condition	N []	E_{opt} (mJ)	E_{arc} (mJ)	E_{gl} (mJ)	Dur. (ms)	E_t (mJ)	η_p []	η_s []	E_{opt}	E_{arc}	E_{gl}	Dur.
Speed	0 m/s	37	2.0	2.8	15.5	2.32	18.3	0.66	0.11	1.02	1.28	1.51	0.15
	1.9 m/s	9	3.7	2.0	16.2	2.18	18.2	0.66	0.21	0.80	0.66	1.31	0.18
	3.8 m/s*	8	5.4	1.8	16.3	1.62	18.1	0.65	0.30	0.70	0.45	1.38	0.03
	5.9 m/s	8	6.7	2.1	16.6	1.42	18.7	0.68	0.36	0.78	0.47	0.81	0.06
Gap	1.0 mm*	8	5.4	1.8	16.3	1.62	18.1	0.65	0.30	0.70	0.45	1.38	0.03
	2.0 mm	9	9.1	2.9	15.4	1.26	18.3	0.66	0.50	0.56	0.33	0.64	0.05
	3.0 mm	8	9.7	3.7	13.2	1.00	16.9	0.61	0.57	0.81	0.33	0.77	0.06
Dia.	0.5 mm	8	8.1	1.4	16.2	1.44	17.6	0.64	0.46	0.40	0.16	0.83	0.05
	1.5 mm	8	7.1	0.6	17.1	1.50	17.7	0.64	0.40	0.35	0.20	0.55	0.04
	2.0 mm*	8	5.4	1.8	16.3	1.62	18.1	0.65	0.30	0.70	0.45	1.38	0.03
Charge	1.5 ms	9	3.6	2.3	8.84	1.04	11.1	0.65	0.32	0.66	0.54	0.99	0.09
	2.0 ms*	8	5.4	1.8	16.3	1.62	18.1	0.65	0.30	0.70	0.45	1.38	0.03
	3.0 ms	6	9.6	1.5	30.8	2.44	32.4	0.58	0.30	1.43	0.42	0.83	0.10
Gas	air*	37	2.0	2.8	15.5	2.32	18.3	0.66	0.11	1.02	1.28	1.51	0.15
	$N_2 + C_3H_8$	12	2.2	0.6	16.3	2.68	16.9	0.61	0.13	0.41	0.09	0.54	0.11
Press.	1 bar*	37	2.0	2.8	15.5	2.32	18.3	0.66	0.11	1.02	1.28	1.51	0.15
	2 bar	7	3.0	2.2	16.4	2.06	18.6	0.67	0.16	0.52	0.61	0.73	0.09
	3 bar	6	4.1	2.4	17.7	2.20	20.1	0.73	0.21	1.13	0.38	1.80	0.29
	4 bar	7	5.0	3.6	16.2	2.11	19.9	0.72	0.25	0.55	0.23	0.75	0.14
	5 bar	9	5.5	4.3	16.0	1.86	20.3	0.74	0.27	0.84	0.26	0.94	0.24
	6 bar	8	5.1	5.6	14.4	1.78	20.0	0.73	0.25	0.70	0.28	0.73	0.16

$\eta_{arc} = 0.20$ and $\eta_{gl} = 0.10$. These estimates are based on relatively small samples considering the variability of the sparks. A more accurate determination of these efficiencies, particularly the arc phase one, would require a larger number of measurements. Saggau [15] gives an efficiency value of 38% for a 2 mJ arc discharge under similar conditions without flow.

For modelling purposes, as a first approximation, the energy input (vs. time) from the spark to the gas can be characterised by a curve like that of Figure 3: an input of $\eta_{arc}E_{arc}$ over a period of several microseconds followed by a period lasting t milliseconds with a constant power equal to $(\eta_{gl}E_{gl})/t$. For the conditions of the experiments presented here, E_{arc}, E_{gl} and t may be taken from Table 3.

CONCLUSION

We have presented a technique based on phase-stepping holographic interferometry for measurement of the energy transfer from a spark to the surrounding gases. This technique enabled us to measure precisely the energy transfer with flow speeds of from 0 to 6 meters per second at the spark gap. Measurements were made for a number of spark plug electrode geometries, pressures and gas speeds with a standard coil ignition system.

- Increasing the flow speed from 0 to 2 meters per second doubles the energy transfer efficiency from the spark to the surrounding gas. With a flow speed of 5 meters per second the efficiency is 3 times that with no flow for the conditions studied (2 millimeter diameter electrodes, 1 millimeter gap, 18 millijoules coil secondary energy).
- We measured spark efficiencies [(energy in gas after spark)/(electrical energy supplied to electrodes)] of from 20 to 60 percent. The values we measured without flow were twice those reported previously for similar conditions.
- We estimate the spark efficiency to be roughly 60% for conditions like those in an engine.
- We have shown how it is possible to estimate the energy transfer efficiencies for the arc and glow phases of the spark based only on measurements of the total energy transferred. Using this technique, we estimated these efficiencies each to be 30% for the conditions studied.

While we were limited in this study to observing the effects of pressure and gas flow speed separately, it should be possible with this technique to measure the spark efficiency in conditions close to those in a motor, i.e. in flowing gases with moderate pressures and temperatures and commercial spark plugs.

ACKNOWLEDGEMENTS

This work was supported in part by the *Groupement Scientifique Moteurs* (*SA*, *Renault* and *IFP*). Technical assistance was provided by M. B. Fonteneau, Dipl. Ing. Messrs J. Hyvönen, P. Lessart and J. Bonnard. The author is also indebted to M. J. F. LeCoz for assistance and a number of discussions on topics related to this project.

REFERENCES

1 Ziegler G.F.W., E.P. Wagner, B. Saggau and R. Maly (1984), Influence of a breakdown ignition system on performance and emission characteristics. *SAE Paper*, 840992.

2 Pischinger S. and J.B. Heywood (1990), How heat losses to the spark plug electrodes affect flame kernel development in and spark-ignition engine. *SAE Paper*, 900021.

3 Douaud A., G. de Soete and C. Henault (1983), Experimental analysis of initiation and development of part-load combustions in spark-ignition engines. *SAE Paper*, 830338.

4 Ko Y., R.W. Anderson and V.S. Arpaci (1991), Spark ignition of propane-air mixtures near the minimum ignition energy: part I. an experimental study. *Combustion and Flame*, **83**, pp. 75-87.

5 Cho Y.S, D.A. Santavicca and R.M. Sonntag (1992), The effect of spark power on spark-ignited flame kernel Growth. *SAE Technical Paper Series*, 922168.

6 Maly R. (1984), Spark ignition: its physics and effect on the internal combustion engine. *Fuel Economy: Road Vehicles Powered by Spark Ignition Engines*, Chapter 3, Eds. J.C. Hilliard, G. S. Springer, Plenum Press.

7 Maly R., B. Saggau, E. Wagner and G. Ziegler (1983), Prospects of ignition enhancement. *SAE Technical Paper*, *Series* 830478.

8 Anderson R.W. and J.R. Asik (1985), Lean air-fuel ignition system comparison in a fast-burn engine. *SAE Technical Paper*, *Series* 850076.

9 Nakai M., Y. Nakagawa, K. Hamai and M. Sone (1985), Stabilized combustion in a spark ignited engine through a long spark duration. *SAE Technical Paper*, *Series* 850075.

10 Kalghatgi G.T. (1987), Spark ignition, early flame development and cyclic variation in I.C. Engines. *SAE Paper*, 870163.

11 Boudier P., S. Henriot, T. Poinsot and T. Baritaud (1992), A model for turbulent flame ignition and propogation in spark ignition engines. *Twenty-Fourth Symposium (Intl) on Combustion,* The Combustion Institute, pp. 503-510.

12 Shen H., P.C. Hinze and J.B. Heywood (1994), A model for flame initiation and early development in SI-engine and its application to cycle-to-cycle variations. *SAE Paper*, 942049.

13 Anbarasu M., D.L. Abata and P.C. Moilanen, Modeling of pressure rise and flame growth in a spark ignition engine. *SAE Paper*, 941930.

14 Teets R.E. and J.A. Sell (1988), Calorimetry of ignition sparks. *SAE Technical Paper, Series* 880204.

15 Saggau B. (1981), Kalorimetrie der drei entladungsformen des elektrischen zündfunkens. *Archiv für Electrotechnik*, **64,** pp.229-235.

16 Roth W., P.G. Guest, Guenther von Elbe and B. Lewis (1951), Heat generation by electric sparks and rate of heat loss to electrodes. *The Journal of Chemical Physics*, **12**, 19, pp. 1530-1535.

17 Kumagai S., T. Sakai and N. Yasugahira (1972), Calorimetry of spark energy. *Combustion Science and Technology*, **6**, pp. 233-239.

18 Merrit L.R. (1978), A spark calorimeter. *J. Phys. E: Sci. Instrum.*, **11**, pp. 193-194.

19 Dändliker R. and R. Thalmann (1985), Heterodyne and quasi-heterodyne holographic interferometry. *Opt. Engr.*, **5**, 24, pp. 824-831.

20 Hariharan P. (1985), Quasi-heterodyne holographic interferometry. *Opt. Engr.*, **4**, 24, pp. 632-638.

21 Verhoeven D. (1993), Simplified phase-shifting holographic interferometry, in optical diagnostics in: *Fluid and Thermal Flow, Soyoung S. Cha, James D. Trolinger, Editors, Proc. SPIE 2005*, pp. 546-552.

22 Beach K.W, R.H. Muller and C.W. Tobias (1973), Light deflection effects in the interferometry of one-dimensional refractive index fields. *J. Opt. Soc. Am.*, **5**, 63, pp. 559-566.

23 Creath K. (1991), Phase-measurement interferometry: beware these errors in: *Laser Interferometry IV: Computer-Aided Interferometry, Ryszard J. Pryputniewicz, Editor, Proc. SPIE 1553,* pp. 213-220.

Final manuscript received in June 1997